J. Fluid Mech. (2024), *vol*. 983, A40, doi:10.1017/jfm.2024.176

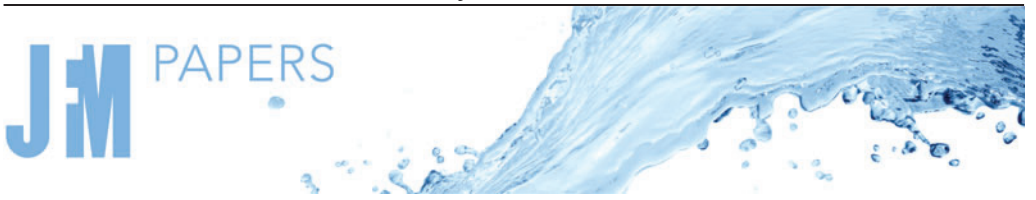

Polydispersity effect on dry and immersed granular collapses: an experimental study

Oscar Polanía[1,2,†], Nicolas Estrada[1,†], Emilien Azéma[2,3,†], Mathieu Renouf[2,†] and Miguel Cabrera[4,†]

[1]Department of Civil and Environmental Engineering, Universidad de los Andes, Bogotá, Colombia

[2]LMGC, Université de Montpellier, CNRS, Montpellier, France

[3]Institut Universitaire de France (IUF), Paris, France

[4]Department of Geoscience & Engineering, TU Delft, Delft, The Netherlands

(Received 17 July 2023; revised 19 February 2024; accepted 20 February 2024)

The column collapse experiment is a simplified version of natural and industrial granular flows. In this set-up, a column built with grains collapses and spreads over a horizontal plane. Granular flows are often studied with a monodisperse distribution; however, this is not the case in natural granular flows where a variety of grain sizes, known as polydispersity, is a common feature. In this work, we study the effect of polydispersity, and of the inherent changes that polydispersity causes in the initial packing fraction, in dry and immersed columns. We show that dry columns are not significantly affected by polydispersity, reaching similar distances at similar times. In contrast, immersed columns are strongly affected by the polydispersity and packing fraction, and the collapse sequence is linked to changes of the basal pore fluid pressure P. At the collapse initiation, negative changes of P beneath the column produce a temporary increase of the column strength. The negative change of P lasts longer in polydisperse columns than in monodisperse columns, delaying the collapse sequence. Conversely, during the column spreading, positive changes of P lead to a decrease of the shear strength. For polydisperse collapses, the excess of P lasts longer, allowing the material to reach farther distances, compared with the collapses of monodisperse materials. Finally, we show that a mobility model that scales the final runout with the collapse kinetic energy remains true for different polydispersity levels in a three-dimensional configuration, capturing the scaling between the micro to macro controlling features.

Key words: avalanches, gravity currents, particle/fluid flow

† Email addresses for correspondence: os.polaniao@uniandes.edu.co, oscar.polania@umontpellier.fr, n.estrada22@uniandes.edu.co, emilien.azema@umontpellier.fr, mathieu.renouf@umontpellier.fr, m.a.cabrera@tudelft.nl

1. Introduction

Granular flows are found in geophysical mass flows such as landslides, debris or pyroclastic flows, or in processes related to the pharmaceutical, food or construction industries. These flows can be subaerial or occur within a fluid (e.g. water), where grain–fluid interactions influence their behaviour. Courrech du Pont *et al.* (2003) classified granular flows into three flow regimes that depend on the dimensionless numbers $St = (\rho_s\,\Delta\rho\,g d^3)^{1/2}/(18\mu_f\sqrt{2})$ and $\chi = \sqrt{\rho_s/\rho_f}$, where d is the grain diameter, g is the gravitational acceleration, μ_f is the fluid dynamic viscosity, and $\Delta\rho = \rho_s - \rho_f$ is the difference between the grain density ρ_s and fluid density ρ_f. The three flow regimes are: the free-fall regime, where ambient drag is negligible ($St \gtrsim 10$ and $\chi \gtrsim 4$); the inertial regime, where grain–fluid interactions depend on the fluid inertia ($St/\chi \gtrsim 2.5$ and $\chi \lesssim 4$); and the viscous regime, where grains are limited by the Stokes velocity ($St/\chi \lesssim 2.5$ and $St \lesssim 10$). In immersed granular flows, the packing fraction $\phi = V_s/V$, quantified as the ratio between the volume V_s of solids and a reference volume V (which could be a total or a local volume), is a feature of major importance because the magnitude of the drag force depends on it (Di Felice 1994). Granular flows are commonly studied with a monodisperse distribution of grains. However, the variety of grain sizes found in nature and industrial applications, known as polydispersity, is an important characteristic (Prada-Sarmiento *et al.* 2019). Increasing the polydispersity level results in an increase of ϕ (Nguyen *et al.* 2014; Oquendo-Patiño & Estrada 2022), leading to denser systems and consequently to flows with stronger grain–fluid interactions (Sufian *et al.* 2019).

The shear strength of a fluid-saturated granular deposit is controlled by the effective normal stresses σ' sustained by the grains. This effective stress is the difference between the total stress acting on the granular system and the pore fluid pressure P. A sudden increase of P, meaning a decrease of σ', can trigger a local instability, with the potential of transforming it into an avalanche. Positive ΔP changes in the pore pressure could follow, among other things, the infiltration of rainwater or changes in the granular packing. For instance, contractions in a granular system produce an excess of pore pressure, or a positive ΔP, expelling fluid from the granular structure, weakening the deposit, and enhancing a collective flow. In contrast, stabilisation is expected to be controlled by dilatancy and the reduction of pore pressure, equivalent to a negative ΔP (Iverson 1997, 2005). Rondon, Pouliquen & Aussillous (2011) showed that contraction and dilatancy in loose and dense granular systems, respectively, influence the initiation of granular flows. In loose systems, contractions produce a temporary increase of the pore pressure that results in fast flows. By contrast, dense granular systems need to dilate, inducing a temporal negative pore pressure change that increases the effective stress and delays the flow. A stable flow is then reached when the changes in the pore pressure stabilise, $\Delta P \simeq 0$, having grains that move in constant friction with the base. Contrariwise, excess pore pressure results in a fluidised flow without shear strength where grains may collide with the base but remain suspended (Ilstad *et al.* 2004). Moreover, the excess pore pressure has been identified as the driving mechanism behind long runout distances in submarine debris flows (Gee *et al.* 1999).

A benchmark experiment for studying granular flows is the collapse of a granular column. In this configuration, a pile of grains with initial length L_0 and height H_0, having aspect ratio $A = L_0/H_0$, is allowed to collapse by self-weight over a horizontal plane. In this experiment, the column collapse initiates with an acceleration stage, followed by a stage of lateral spreading with nearly constant velocity U, until the flow decelerates and stops. When the collapse comes to a halt, a final deposit with maximum height H_f and runout L_f describes the final geometry (Staron & Hinch 2005; Meruane, Tamburrino &

Roche 2010; Bougouin, Lacaze & Bonometti 2017). The mobility of granular columns, also understood as the flow runout distance L_f, or its normalised form $L^* = (L_f - L_0)/L_0$, is a major characteristic that represents the frictional strength on a macro scale (Staron & Hinch 2007). Studies have shown that L^* increases and scales with A for different flow regimes, distinguishing between short and tall columns (Balmforth & Kerswell 2005; Roche *et al.* 2011; Warnett *et al.* 2014; Pinzon & Cabrera 2019). This distinction arises from the collapse sequence. While short columns slide laterally from the collapse initiation, tall columns (i.e. for $A \gtrsim 2$) show dominant free-fall before spreading horizontally. In immersed columns belonging to the viscous regime, the relative increase in the initial packing fraction ϕ_0 of monodisperse columns plays an important role in the flow behaviour, influencing the collapse initiation and mobility. Dense columns ($\phi_0 \gtrsim 0.60$) are delayed due to the flow of fluid into the granular structure during dilation. This process produces a negative change in the pore pressure that temporarily increases the column strength, and as a result of this, dense columns have a slower collapse process and have shorter mobility than loose ones (Rondon *et al.* 2011; Wang *et al.* 2017; Yang *et al.* 2020; Lee 2021). The effect of ϕ_0, although significant in viscous flows, tends to disappear for other regimes (Lacaze *et al.* 2021). The effect of pore pressure changes on the collapse initiation has been well identified, but it represents only the initial stage of the collapse process, and the role of pore pressure in the propagation phase remains unexplored.

Grain size segregation is an intrinsic phenomenon in granular materials under shear, developing when differences in size or density are found in the constituent grains (Gray & Ancey 2011). Previous works have shown that the mobility of bidisperse granular columns increases due to a segregation layer (Roche *et al.* 2005; Phillips *et al.* 2006; Meruane, Tamburrino & Roche 2012). This effect is enhanced when the size ratio between big and small grains increases, and when the column is immersed (He, Shi & Yu 2021). The mobility of columns is also affected by the heterogeneity of grain layers of different sizes, leading to an increase in the runout distance of initially segregated columns (Degaetano, Lacaze & Phillips 2013; Martinez *et al.* 2022). For polydisperse systems, numerical studies have indicated that mobility increases with polydispersity (Watanabe, Moriguchi & Terada 2022) and have suggested that small grains enhance mobility because they lubricate the system (Lai *et al.* 2017). However, it was found that the lubrication mechanism is a biased interpretation of small system to grain size ratio, showing that the mobility, which represents the frictional strength, of dry granular columns is independent of polydispersity (Cabrera & Estrada 2021). The latter result, in the granular column configuration, is in agreement with previous studies that have shown the independence of the shear strength of polydisperse granular materials when they reach a residual stage at large deformation (Nguyen *et al.* 2015; Cantor *et al.* 2018; Cantor, Azéma & Preechawuttipong 2020; Polanía *et al.* 2023). The effect of polydispersity on immersed granular flows has been studied less, but it has been shown with a numerical approach that the collapse of immersed columns is delayed with an increase in the polydispersity level (Polanía *et al.* 2022). Despite these previous works, the effect that polydispersity has on immersed granular columns remains insufficiently investigated, especially experimentally.

In the study of granular flows, mobility models provide a simplified interpretation of a complex process. These models relate granular flows of different scales to the initial and flow conditions, considering the column initial geometry and collapse kinematics. Although simple, the scaling between the column mobility and the aspect ratio is a mobility model that comes from the force balance between the basal friction force and the normal force of the moving mass (Lajeunesse, Monnier & Homsy 2005). Other studies have shown, with numerical simulations, a link between the final runout and the collapse kinematics at the grain scale (Topin *et al.* 2012) and at the flow scale (Yang *et al.* 2020;

Guo *et al.* 2023). These models work well for flows with monodisperse grains but depend on fitting parameters or flow variables, such as the flow average height, which are difficult to estimate in transitional flows. Polanía *et al.* (2022) proposed a simplified model that links the column mobility to the collapse kinetic energy. This model, which relies entirely on physically based variables, does not need fitting parameters and works for different levels of polydispersity, has not yet been verified experimentally.

Our study presents experimental evidence on how polydispersity and the packing fraction affect the collapse sequence and mobility of dry and immersed granular columns that are in the free-fall and inertial regimes, respectively. The experiments involve columns consisting of glass beads of different sizes, and allow the study of monodisperse and polydisperse systems. We use glass beads in order to avoid undesirable effects such as grain elongation, angularity or rugosity, allowing us to focus only on the influence that the grain size distribution – and, intrinsically, the packing fraction – has on granular flows. We captured the basal pore pressure beneath the column initial geometry and along the collapse principal direction. We link the evolution of the pore pressure to the sequence of the column collapse, and reveal how these two are influenced by increasing polydispersity level. Finally, we test whether the link between the collapse kinetic energy and mobility, introduced by Polanía *et al.* (2022), remains true in three-dimensional polydisperse collapses.

2. Collapse experiments

We conducted the column collapse experiments in a rectangular glass channel that was 100 cm long, 60 cm high and 18 cm wide, in dry and immersed conditions. For immersed experiments, we used tap water with density $\rho_w \simeq 1000$ kg m^{-3} and dynamic viscosity $\mu_w \simeq 0.001$ Pa s, up to a level of $H_w \simeq 50$ cm. The granular columns had initial length $L_0 \simeq 8.5$ cm and initial height $H_0 \simeq [4.2, 8.5, 17, 24]$ cm, allowing the study of short and tall columns with aspect ratios $A \simeq [0.5, 1, 2, 2.8]$. A novelty of our study is the releasing mechanism of the granular column, for which we placed an acrylic gate that was 18 cm wide and 0.8 cm thick at L_0, and covered it with a 0.05 cm thick and 15.24 cm wide PTFE film. One end of the PTFE film was fixed to a roller, and the other end, facing the granular column, had displacement restraints. A motor rotated the roller and pulled the PTFE film from one end, removing the gate vertically with velocity $V \simeq 0.85$ m s^{-1}. This mechanism reduces the effects generated by the relative displacement of the gate and the grains as they are not in direct contact (see figure 1). In all cases $V > 0.4\sqrt{gH_0}$, meaning that the gate uplift velocity did not influence the column collapse (Sarlin *et al.* 2021).

We defined the polydispersity level, $\lambda = d_{max}/d_{min}$, as the ratio between the maximum and minimum grain diameters (d_{max}, d_{min}) and studied four values of $\lambda = [1.0, 3.8, 12.6, 20.0]$. The samples' grain size distribution (GSD) had a cumulative volume fraction (CVF) that followed a power law of the form CVF $= (d/d_{max})^n$. For each λ, we chose an exponent $n = [1, 1.38, 0.69, 0.47]$, having a common CVF of 0.5 at $d_{50} = 1.15$ mm. We used these GSDs to build samples having an initial packing fraction of $\phi_0 \simeq [0.64, 0.68, 0.75, 0.76]$, studying dense columns with ϕ_0 comparable to or exceeding the value for the random close packing of monodisperse spheres, $\phi_{rcp} \simeq 0.64$ (Scott 1960) (see figure 2). We used silica-lime glass beads with density $\rho_s = 2500$ kg m^{-3} produced by Sigmund Linder GmbH.

Under the flow regime classification proposed by Courrech du Pont *et al.* (2003), the immersed collapse experiments conducted in this study are considered as being in the inertial regime with $St = 9.28$ and $\chi = 1.58$. For dry column collapses, we assumed

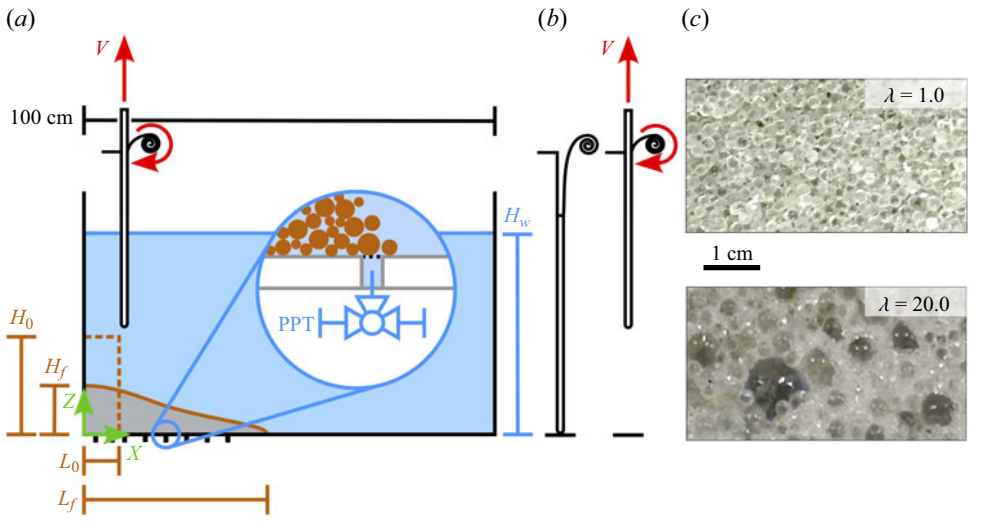

Figure 1. Sketch of the column collapse experimental set-up. (*a*) Side view highlighting the column initial and final heights and lengths (H_0, L_0) and (H_f, L_f), respectively. Note that $L_0 \simeq 8.5$ cm for all experiments, and for immersed collapses the water level is $H_w \simeq 50$ cm. The inset shows the set-up for the basal pore pressure transducer (PPT) placed at $X = [3, 7, 10, 15, 20, 25, 30, 35]$ cm and $Y = 9$ cm. (*b*) The release mechanism. The column collapses after removing a gate vertically with velocity $V \simeq 0.85$ m s^{-1}. The gate is pulled by rapidly rolling a PTFE film, reducing shear on the face contacting the grains. (*c*) Close-up lateral views of the glass bead granular systems with size ratios $\lambda = d_{max}/d_{min} = 1$ and 20, where d_{min} and d_{max} are the minimum and maximum grain diameters, respectively.

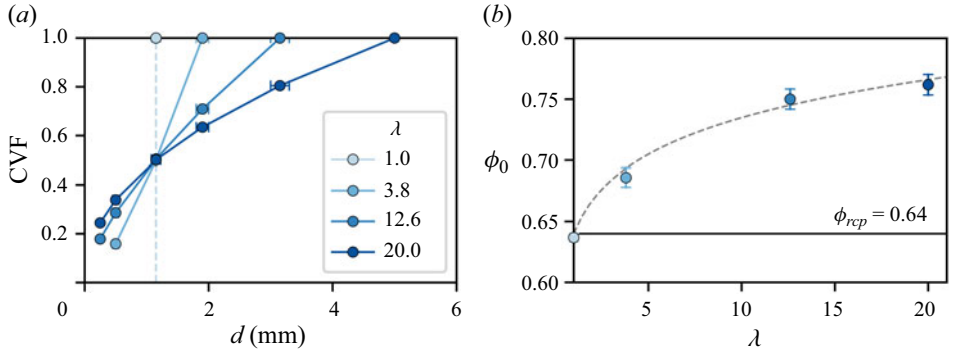

Figure 2. (*a*) The CVF as a function of the grain diameter d with a distribution following CVF $= (d/d_{max})^n$ with $n = [1, 1.38, 0.69, 0.47]$ for the size ratios $\lambda = [1, 3.8, 12.6, 20]$, respectively. All GSDs have common CVF 0.5 for $d_{50} = 1.15$ mm. Markers represent the mean size, and horizontal bars represent the ranges in size reported by the supplier. (*b*) Average sample initial packing fraction ϕ_0 as a function of λ. The vertical error bars represent the variability among samples with the same polydispersity level. The dashed line follows a power-law function in the form $\phi_0 = \lambda^{0.06}\phi_{rcp}$, with ϕ_{rcp} being the random close packing of monodisperse spheres (Scott 1960).

air density to be $\rho_a = 1.2$ kg m^{-3} and viscosity to be $\mu_a = 1.8 \times 10^{-5}$ Pa s, having experiments classified in the free-fall regime with $St = 662.60$ and $\chi = 45.18$. We considered d_{50} as the characteristic flow diameter for all polydispersity levels. In our experiments, the ratios L_0/d_{50} and W_{ch}/d_{50}, with $W_{ch} = 18$ cm being the channel width,

are sufficiently large, and the experiments are not affected by grain size (Cabrera & Estrada 2019) or side-wall effects (Jop, Forterre & Pouliquen 2005).

We recorded the column collapse with a Motionblitz-cube-4 high-speed camera. The experimental set-up was backlit with an LED panel, improving the image contrast and allowing better recognition of the moving mass. The post-processing of the digital images included a perspective correction with known coordinates at the front wall inside the channel. We measured fluid pressures at the channel base with a series of eight pore pressure transducers (PPTs). The channel base is perforated with eight holes of diameter 10 mm centred at $X = [3, 7, 10, 15, 20, 25, 30, 35]$ cm. In these holes, a 6 mm hose was inserted and sealed with silicon. The hose is connected to a three-way ball valve, allowing the hose to purge for removing air bubbles, on one end, and on the other end is a connection with the PPT. The hose free tip, the one inside the channel, is covered with a mesh with openings of 0.075 mm that stops grains from flowing through the hose (see figure 1). The PPTs were of the type 26PCCFA6D produced by Honeywell, and they were tested and calibrated for a fluid pressure range of $P \in [98, 4900]$ Pa. Both the high-speed camera recordings and the PPT measurements were registered at sampling frequency 500 Hz.

To reduce segregation during the construction of the granular column, and to have the best possible homogeneous sample, we found it satisfactory to hand-mix the grains in a wide bowl and then gently pour the mix into a grid of six rectangles inside the channel. Once the grid was filled, it was pulled up and laid over the grain layer, and then the channel was knocked gently to densify the sample. We repeated this process until the desired H_0 was reached. In order to avoid having air inside the granular column in immersed experiments, we went through the same process with an increasing water level, enough to cover the grid.

An experiment started with initiating the PPTs and camera recording. Then we triggered the releasing gate and let the column collapse by self-weight. When the collapse came to a halt, we measured directly the deposit final runout L_f and height H_f. For immersed experiments, we drained the channel, removed the grains, and let them dry over 24 h in an oven at 100 °C. Once the grains were dry, or simply removed from the channel after a dry experiment, we sieved them and prepared them for another experiment. In order to quantify the experiment's repeatability, we conducted two repetitions for certain combinations (A, λ) and found consistent results between them. A table summarising the experiments conducted can be found in the supplementary material available at https://doi.org/10.1017/jfm.2024.176.

3. Collapse sequence

After removing the gate, the column starts to collapse, releasing a wedge of grains that moves vertically and then spreads horizontally. For dry columns, polydispersity plays a minor role in the collapse sequence. The mobilised masses of monodisperse and polydisperse columns have similar heights and reach similar horizontal distances almost at the same time (see figure 3*a*,*b*). For immersed cases, the first stage of the column collapse reveals differences between monodisperse and polydisperse columns, showing that systems with $\lambda = 1$ collapse faster than systems with $\lambda = 20$ (see figure 3*c*,*d*). An important aspect of polydisperse columns is the initial vertical fall of grains at the column releasing face, while the core remains still. High packing fractions, due to high polydispersity levels, frustrate the rapid percolation of water into the granular structure and produce a retrogressive collapse mechanism. Similar collapse mechanisms have been observed for sand columns (Thompson & Huppert 2007) and polydisperse columns in

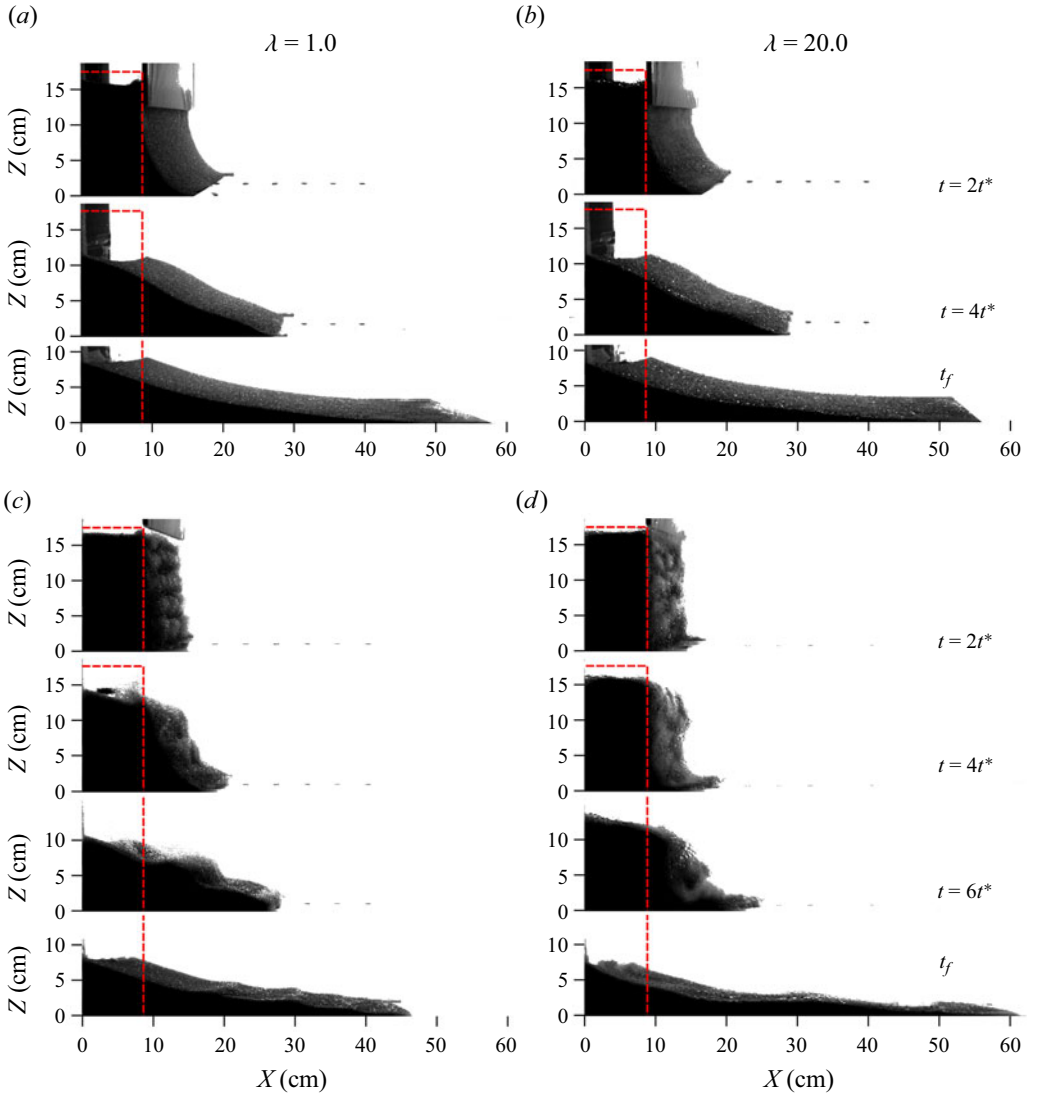

Figure 3. Collapse sequence of (*a*,*b*) dry and (*c*,*d*) immersed columns with aspect ratio $A = H_0/L_0 \simeq 2$ and with (*a*,*c*) $\lambda = 1$ and (*b*,*d*) $\lambda = 20$. The red dashed lines indicate the column initial geometry; $t^* = \sqrt{H_0/g^*}$ is a characteristic column time, where $g^* = g\,\Delta\rho/\rho_s$ is a scaled gravity due to the ambient fluid, with $\Delta\rho = \rho_s - \rho_f$ being the difference between ρ_s and ρ_f, the solid and fluid densities.

two-dimensional simulations (Polanía *et al.* 2022). The motion of monodisperse collapses finishes earlier than that of polydisperse collapses, resulting in longer runout distances for systems with $\lambda = 20$ than for $\lambda = 1$. The final deposits of immersed collapses have a wavy shape that is produced by strong grain–fluid interactions on the surface of the moving mass. In contrast, due to the negligible air viscosity, the deposits of dry collapses have a smooth surface. The collapse sequence in figure 3 presents the collapse evolution at equivalent moments for a time scale normalised by a characteristic time $t^* = \sqrt{H_0/g^*}$, where $g^* = g\,\Delta\rho/\rho_s$ is a scaled gravity due to the ambient fluid (see the movies in the supplementary material).

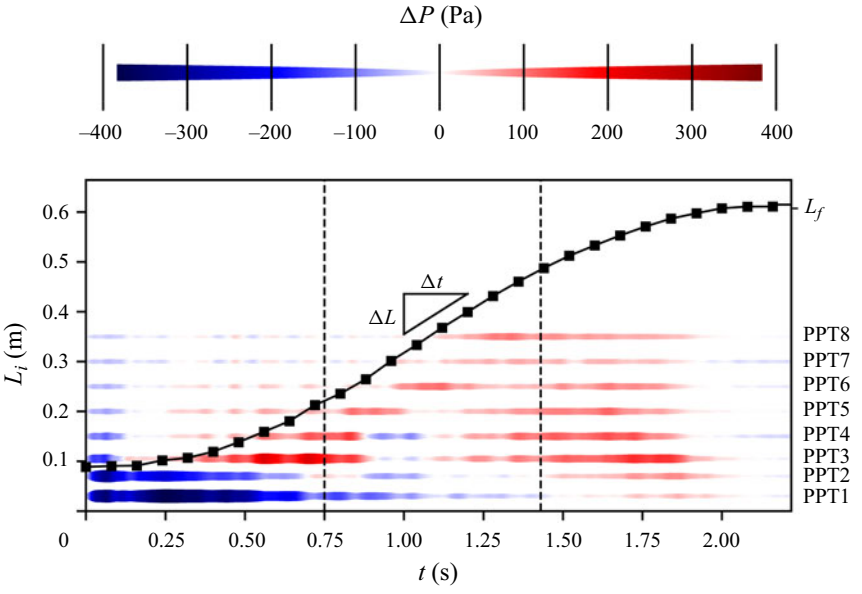

Figure 4. Evolution of the front position $L(t)$ and fluid pressure change ΔP for a column with $A \simeq 2$ and $\lambda = 20$. The fluid pressure change is computed as $\Delta P(t) = P(t) - P_0$, where $P(t)$ is the pressure registered by the PPTs and P_0 is the initial hydrostatic pressure. Note that only PPT1 and PPT2 are beneath the column initial geometry. The dashed lines indicate the instants when the collapse reaches $L_{25} = L_0 + 0.25(L_f - L_0)$ and $L_{75} = L_0 + 0.75(L_f - L_0)$, which delimit the collapse steady propagation stage interval where the front velocity U is computed.

From the recorded digital images, we obtained the moving mass height profile during the entire collapse sequence in the (X, Z) plane and the front position evolution $L(t)$, both measured at the front wall. Changes of the pore pressure are monitored as $\Delta P(t) = P(t) - P_0$ during the column collapse, where $P_0 = \rho_w g H_w$ is the initial hydrostatic pressure. The information on $L(t)$ and $\Delta P(t)$ allows us to link the effect that one has on the other during the collapse sequence (see figure 4). We present this link in § 3.3 only for immersed columns because in our experiments the pressure changes induced by dry flows were negligible.

3.1. *Role of polydispersity and packing fraction*

The evolution of the front position for dry collapses shows that increasing the level of polydispersity λ has a minor effect on the collapse sequence. Regardless of λ, collapses exhibit notable differences neither at the collapse initiation nor during the spreading stage. The front position of dry collapses reaches similar distances at similar times, revealing the flow independence with respect to the GSD during the constant shearing of the moving mass. At the end of the collapse, the final runout increases roughly with the polydispersity λ (see $L(t)$ for dry collapses in figure 5*a*). In contrast, the collapse sequence of immersed columns depends on the polydispersity level and, intrinsically, on the initial packing fraction. Notably, polydispersity affects the collapse initiation and the final runout. Note in figure 5(*a*) that the horizontal spreading of immersed columns with $\lambda = 20$ is delayed compared with columns with lower polydispersity. The delay of the horizontal spreading in polydisperse systems, induced by the large initial packing fraction, is in agreement with previous studies (Pailha, Nicolas & Pouliquen 2008; Rondon *et al.* 2011).

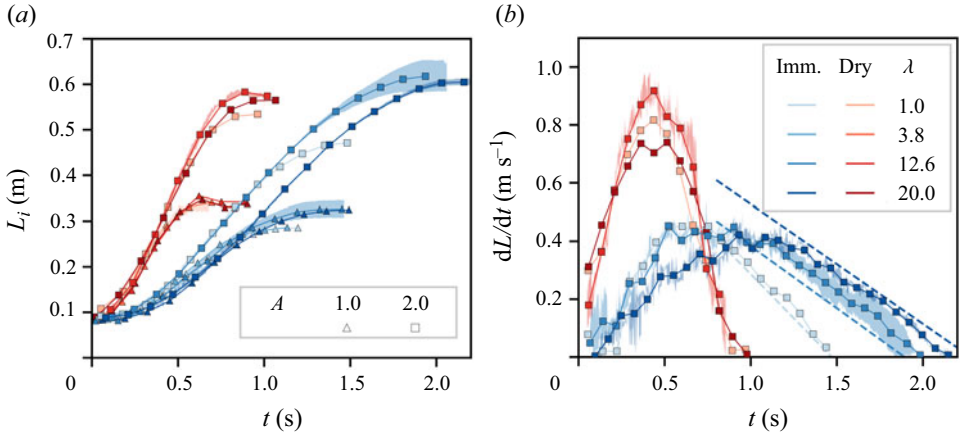

Figure 5. (*a*) Front position evolution $L(t)$ for dry (red) and immersed (blue) columns, and for $A \simeq 1$ (△) and $A \simeq 2$ (□). (*b*) Front velocity evolution dL/dt for dry and immersed columns with aspect ratio $A \simeq 2$. Shaded areas represent the variability between repetitions, with envelopes indicating the minimum and maximum values, and markers and continuous lines are the average of them. In (*b*), the dashed lines represent the collapse acceleration magnitudes d^2L/dt^2 for immersed columns during the collapse deceleration phase.

However, despite the consistent increase of the packing fraction with the polydispersity, we observed that collapses were delayed only in samples with the greatest polydispersity ($\lambda = 20$). Interestingly, samples with $\lambda = 12.6$ and 20.0 have similar initial packing fractions, $\phi_0 \sim 0.75$ and 0.76, respectively, but their collapse initiation is considerably different, indicating that the flow initiation is affected not solely by the packing fraction but also by features of the GSD such as the proportion of small grains, which is larger for $\lambda = 20$ (see figure 2).

The time derivative of the front position dL/dt represents the evolution of the front velocity, and the second time derivative d^2L/dt^2 is the front acceleration (see figure 5*b*). Columns have an initial acceleration phase that in dry cases is similar for all polydispersity levels. For immersed columns, the velocity of samples with $\lambda = 20.0$ evolves at a lower rate compared with other polydispersity levels. Then collapses transition to a stage where the peak velocity is reached and – especially for immersed cases – the collapse maintains a nearly steady velocity U. Finally, collapses transition to the deceleration phase where the velocity decreases almost linearly (i.e. constant deceleration). For dry cases, the velocity decreases with a similar rate independently of λ, and collapses stop at similar times. In immersed columns, the deceleration phase depends on the initial packing fraction ϕ_0 and the polydispersity level λ. For instance, monodisperse collapses with $\phi_0 \simeq 0.64$ have a greater rate of velocity loss than the polydisperse collapses $\lambda = 12.6$ and 20.0 with $\phi_0 \simeq 0.75$ and 0.76, respectively, for which the deceleration magnitude is similar.

We found it satisfactory to consider the collapse steady stage between the times when the front had reached $L_{25} = L_0 + 0.25(L_f - L_0)$ and $L_{75} = L_0 + 0.75(L_f - L_0)$ (see figure 4) and consider the steady-state velocity U as the mean velocity on this interval. Figure 6 presents the steady velocity U as a function of H_0 and shows that it is closely related to the theoretical free-fall velocity $U_{ff} = \sqrt{2g^*H_0}$, having good agreement when U_{ff} is scaled by factors of 0.5 and 0.28, which are values typically obtained for column collapses belonging to the free-fall and inertial regimes, respectively (Bougouin & Lacaze 2018). Moreover, U

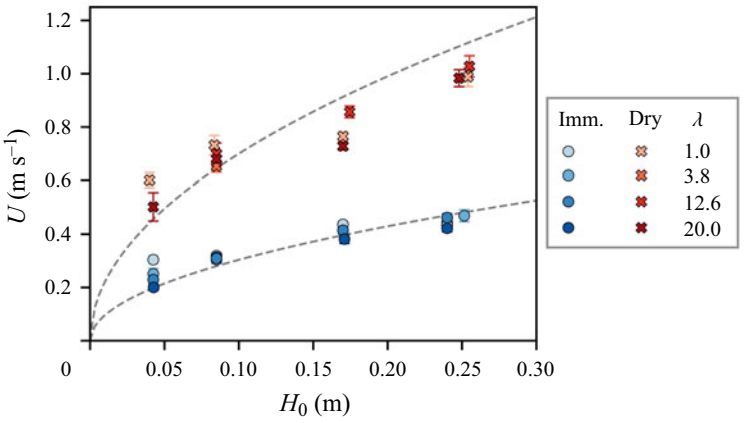

Figure 6. Front velocity U during the steady propagation stage as a function of the column initial height H_0. Results are shown for dry (red) and immersed (blue) columns, and for all values of λ. The dashed lines indicate the theoretical free-fall velocity $U_{ff} = \sqrt{2g^* H_0}$ scaled by factors of 0.50 and 0.28 for dry and immersed columns, respectively. The interval where U is computed is shown in figure 4, and vertical error bars indicate the standard deviation within the interval.

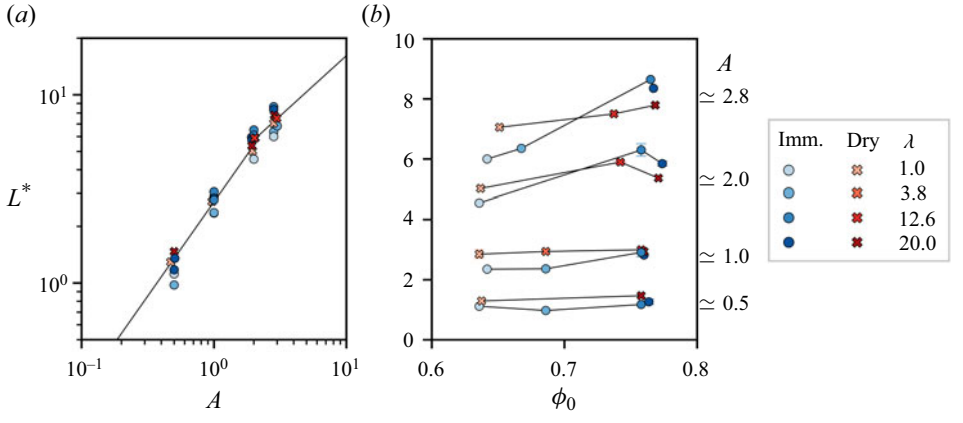

Figure 7. Normalized final runout $L^* = (L_f - L_0)/L_0$ as a function of (*a*) A and (*b*) ϕ_0. The lines in (*a*) indicate $L^* = aA^b$, with the values $(a, b) = (2.7, 1.0)$ for short columns ($A < 2$) and $(a, b) = (3.7, 0.64)$ for tall columns ($A \geq 2$). Error bars indicate variability between repetitions.

has more variability in dry collapses than in immersed collapses and, for the latter, U is marginally affected by λ with a slight reduction for $\lambda = 20$.

3.2. *Column runout*

The mobility of a granular column increases with the aspect ratio A and follows a power-law function in the form $L^* = aA^b$ (Lube *et al.* 2004; Zenit 2005). Our results can be fitted by the coefficients $(a, b) = (2.7, 1)$ for short columns and $(a, b) = (3.7, 0.64)$ for tall columns, similar to those found by Bougouin & Lacaze (2018) (see figure 7*a*). However, for immersed columns, the results deviate from the trend because in general the increase of the polydispersity level enhances the column mobility. For instance, the mobility in monodisperse systems is slightly, but consistently, larger for dry columns than

for immersed columns. The increase of the column λ, representing an increase of the column initial packing fraction ϕ_0, boosts the mobility of immersed columns, resulting in final deposits with a longer runout distance even when compared with dry columns. The increase of the column mobility produced by λ and ϕ is enhanced by the column height. In short columns ($A \simeq 0.5$), the runout barely changes with λ for both dry and immersed cases. In contrast – and for the sake of simplicity we compare only the cases of extreme λ – the runout of columns with $\lambda = 20.0$ is longer than the runout of columns with $\lambda = 1.2$, with an increase of between 20 % and 39 % for aspect ratios $A \simeq 1$ and $A \simeq 2.8$, respectively, while in dry cases the runout change is less than 8 % (see figure 7*b*). For immersed columns, the largest runout was obtained consistently for columns with $\lambda = 12.6$, rather than for $\lambda = 20.0$. This suggests a transition from inertial to viscous behaviour due to an increase in the level of polydispersity and its associated proportion of small grains.

Previous studies exploring the effect of ϕ_0 on monodisperse granular columns have demonstrated that the relative increase in the column packing fraction reduces the mobility of columns that belong to the viscous regime (Rondon *et al.* 2011; Wang *et al.* 2017; Lee 2021). We observe that an increase in the column packing fraction, resulting from a higher polydispersity level, favours the mobility of immersed granular columns in the inertial regime. This result offers a new perspective on the influence of polydispersity and packing fraction on granular flows, and leads to questions about the reasons for the reduction of the effective friction strength, equivalent to a larger runout, in such systems. We observed grain size segregation in the deposit in neither dry columns nor immersed columns. Therefore, we cannot attribute to segregation the reason for the increasing runout in highly polydisperse columns, especially in immersed cases. However, we can link features of the collapse sequence, such as the deceleration phase, to changes in the basal pore pressure, thanks to our experimental set-up and instrumentation (see figure 4). In the next subsection, we discuss the relationship between varying levels of polydispersity in immersed collapses and changes in the basal fluid pressure.

3.3. *Basal pore fluid pressure*

We found that there is a link between the evolution of the pore fluid pressure and the collapse sequence, and vice versa. By observing the evolution of the front position, it is possible to demarcate three moments of basal pore pressure changes ΔP. The results presented in figure 4 show clearly those three moments of pore pressure evolution for the case of a column with $A \simeq 2.0$ and $\lambda = 20$ (see figure 3*d*). First, beneath the column initial geometry (i.e. PPT1, PPT2) the pore pressure decreases. It can be assumed that a decrease in pore pressure induces a fluid flow into the granular structure as the dense granular column dilates, resulting in a temporary increase of the effective stress σ' (Rondon *et al.* 2011; Rauter 2021). At this first moment, the PPTs outside the column initial geometry ($X > L_0$) do not record significant pressure changes. Second, during the horizontal spreading stage, the moving mass produces a positive ΔP, indicating that fluid is being expelled from the decelerating granular mass, reducing the void volume and decreasing the effective stress σ'. Note in figure 4 that the amplitude of ΔP increases significantly after the granular front arrives at any of the PPT positions. Then ΔP transitions from positive to negative values, indicating local variations in the deposit packing (e.g. dilation, contraction) and basal slip velocities (Breard, Dufek & Roche 2019), until a state of full dissipation (i.e. $\Delta P \simeq 0$) is reached that coincides with the front position reaching L_f. It is important to note that pore pressure changes are measured even before the moving mass

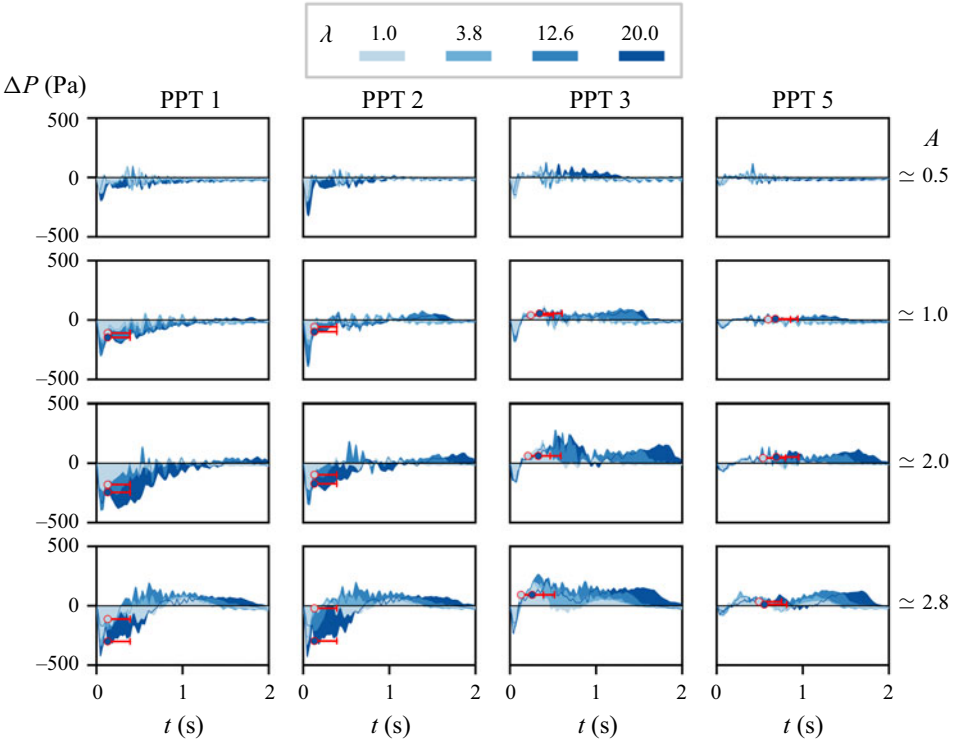

Figure 8. Evolution of ΔP for the PPTs 1, 2, 3 and 5 (columns), for columns with $A \simeq [0.5, 1, 2, 2.8]$ (rows) and for all λ. Markers indicate ΔP at the time when the front reaches the PPTi position for $\lambda = [1, 20]$, and the horizontal red bar indicates an interval of $\bar{t} = 0.25$ s. For PPT1 and PPT2, both beneath the column initial geometry, the horizontal bars indicate the time interval $t = [\bar{t}/2, 3\bar{t}/2]$.

passes over the PPT position. This is due to an increase in the fluid pressure driven by the moving mass, expelling and pushing the fluid as a result of the grain mixture densification and particle–fluid drag interactions (Pinzón & Cabrera 2019).

Let us now compare the effect that λ and A have on the first two moments of ΔP. At the collapse initiation, when the pore pressure changes beneath the column are negative, the amplitude of ΔP increases with A, λ and, intrinsically, ϕ_0. This means that more fluid needs to enter the material pores as it dilates because the column becomes denser with the increase of ϕ_0, and A increases the column's volume. This observation is in agreement with the results of Ahmed, Martinez & DeJong (2023), who showed that polydisperse granular assemblies with large packing fractions develop a greater amplitude of negative pore pressure changes, indicating their tendency to dilate when deforming. Columns with $\lambda = 12.6$ and 20, which have $\phi \simeq 0.75$ and 0.76, respectively, develop the greatest amplitude of negative pore pressure changes ΔP. However, it is interesting to notice that ΔP remains negative with a greater intensity and during a longer period for $\lambda = 20$ even when its packing fraction is very close to the packing fraction of $\lambda = 12.6$. This indicates that in columns with the largest polydispersity level, the fluid flow through them lasts longer (see columns PPT1 and PPT2 in figure 8).

The flow of a fluid through a porous medium, as in the granular columns, can be interpreted as the flow through a network of interconnected pipes controlled by the column hydraulic permeability k. The lower k is, the slower the fluid flow through the column.

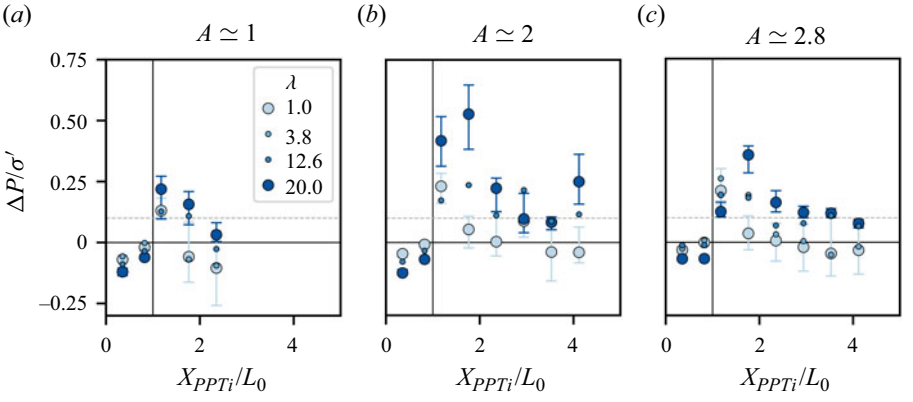

Figure 9. Ratio between the basal pore pressure changes ΔP and the effective stress σ' when the flow front arrives at the position X_{PPTi} for all λ and for columns with $A \simeq [1, 2, 2.8]$. Here, ΔP was taken to be the median value of a 0.25 s interval after the front arrives at X_{PPTi}, and the error bars indicate the first and third quartiles of the same interval. We compute $\sigma' = \phi_0 \rho_p g h_i$ with the average flow height h_i for the same time interval. For for PPT1 and PPT2, both beneath the column initial geometry, ΔP was considered for the time interval $t = [\bar{t}/2, 3\bar{t}/2]$ (see markers in figure 8). The dashed lines indicate $\Delta P/\sigma' = 0.1$.

The permeability k depends on ϕ_0 and the solid-specific surface M_s, and it decreases with an increase of any of the above (Carman 1937). For a sphere of diameter d, the specific surface is $M_s = 6/d$, so a greater fraction of small grains increases M_s and decreases the pore sizes, hindering the fluid percolation through the granular structure. Among our experiments, columns with $\lambda = 20$ have the highest ϕ and the highest concentration of small grains (see figure 2*a*), hence the lowest k. This fact explains that in columns with $\lambda = 20$, the negative change of pore pressure ΔP lasts for a longer period, leading to a slower collapse initiation when compared with columns of lower polydispersity levels (see figure 5).

At the second moment of the pore pressure changes ΔP, the grains' collective movement and the associated void reduction induce positive pore pressure changes after, or in some cases before, the arrival of the front at the PPT position. The peak positive ΔP is recorded at an early stage of the collapse process close to the initial length of the column, and increases for tall columns. At this stage, where the collapse is transitioning mainly from vertical to horizontal motion, the flow could be assumed to be fully fluidised. It is interesting to note that for monodisperse columns ($\lambda = 1$) with $\phi_0 \simeq 0.64$, the positive ΔP peak vanishes rapidly, while for polydisperse columns with larger initial packing fractions, the dissipation of the excess pore pressure lasts longer (see column PPT3 in figure 8).

Figure 9 shows the measurements of pore pressure changes after the front arrives at each PPT as the ratio between the average ΔP obtained for a time interval $\bar{t}$ and the equivalent effective stress σ'. We estimate $\sigma' = \phi_0 \rho_p g h_i$, where h_i is the average collapse height over PPTi during $\bar{t}$, obtained from image analysis. The fluid pressure is averaged over a time interval of $\bar{t} = 0.25$ s, being within a range given by two characteristic times: the time of the column release, $t_g = H_0/V$, and the viscous time in the granular column, $t_v = 18\mu_f H_0/(\Delta\rho\, g d_{50})$ (Bougouin & Lacaze 2018). Considering the height of the tallest column, $H_0 = 0.24$ m, and the material parameters described in § 2, the characteristic time range is $[0.22, 0.28]$ s. Although the PPT measurements are influenced not only by the moving mass but also by the induced fluid fluxes, the average results obtained from them allow a distinction between columns of different λ and ϕ_0. For instance, in

monodisperse columns, the positive peak ΔP rapidly vanishes to $\Delta P \simeq 0$. In contrast, when the columns have high ϕ_0 and low permeability, such as in $\lambda = 12.6$ and 20 with $\phi_0 \simeq 0.75$ and 0.76, respectively, the excess pore pressure dissipation lasts longer, because a large concentration of grains induces greater drag and reduces the depositing velocity (Kaitna *et al.* 2016), producing a localised fluidisation at the base. Figure 9 also includes the average ΔP measured at PPT1 and PPT2, both beneath the column initial geometry but close to the front position when the collapse starts, showing the whole transition that begins with negative ΔP at $X_{PPT} < L_0$ and shifts to positive ΔP at $X_{PPT} > L_0$.

A comparison of two systems with extreme polydispersity levels $\lambda = [1, 20]$ highlights differences in the collapse sequence that can be attributed to differences in the evolution of basal pore pressures. For highly polydisperse columns, positive pore pressure changes reduce σ' for a longer period. The reduction of σ' leads to a decrease of the deceleration magnitude, allowing the moving mass to flow for a longer time, hence resulting in longer runout distances than in monodisperse columns (see figure 5). Our results indicate that when ΔP increases to approximately 10 % of σ', the column collapse can have a prolonged period of spreading (see figure 9). An interesting observation arises when comparing ΔP for systems with $\lambda = 12.6$ and 20, which have $\phi_0 \simeq 0.75$ and $\phi_0 \simeq 0.76$, respectively. For these two polydispersity levels, changes of the basal pore pressure show a similar tendency with $\Delta P/\sigma' \gtrsim 0.1$ beyond the column initial length, leading them to have the lowest deceleration and the greatest mobility. This result suggests that immersed polydisperse granular flows might be better described by an initial packing fraction ϕ_0 rather than by a characteristic grain diameter d (Dahl, Clelland & Hrenya 2003; Breard *et al.* 2020).

4. Mobility model

Previous observations help in integrating the controlling variables of the collapse sequence into a mobility model. Mobility models are a simple yet functional way to estimate the mobility of granular flows. They provide a simplified interpretation of a complex process, and link certain initial and flow conditions to the final column runout. Polanía *et al.* (2022) proposed a simplified model that links the column collapse kinetic energy to the final runout as

$$L^* \propto \frac{1}{L_0}\frac{\rho_p}{\Delta\rho}\sqrt{E_K^U}, \tag{4.1}$$

where $E_K^U = MU^2/2$ is the collapse kinetic energy during the horizontal propagation stage and $M = L_0 H_0 \phi_0 \rho_s$ is the column mass. Here, M is treated as a mass of unitary width, because the column collapse experiment is a width-independent problem. The concept behind the model is an analogy of a sliding block that has an initial velocity and an opposite resistance. By assessing the controlling factors within the model, it was found that the collapse energy E_K^U is the foremost parameter for establishing a relationship between the flow condition and the column final runout that works satisfactorily for free-fall and inertial regime flows. In (4.1), the ratio between ρ_p and $\Delta\rho$ compensates for the difference in velocity U of dry and immersed collapses.

Figure 10 presents the scaling of the normalized final runout L^* with the column kinetics according to (4.1), and shows that results from numerical simulations and experiments follow a similar trend. We validate that this simplified model remains true for columns belonging to the free-fall and inertial regimes. Moreover, we verify the model with the experimental results of Bougouin & Lacaze (2018), who covered a wider range of aspect ratios $A \in [0.2, 9.2]$, confirming the model validity for shorter and taller columns.

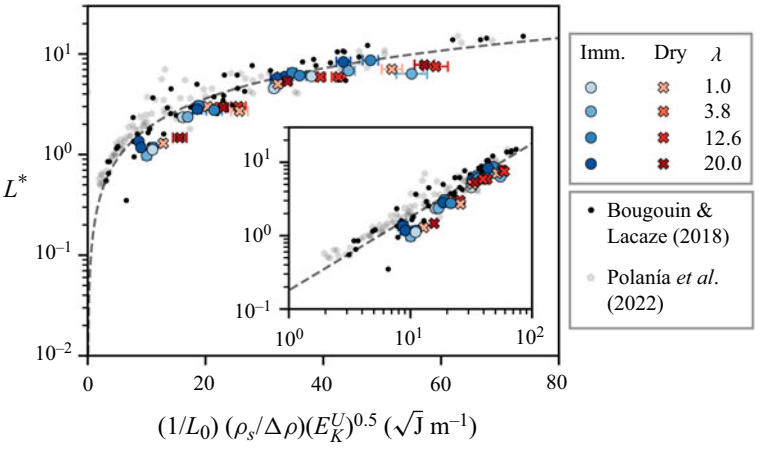

Figure 10. Scaling of the normalized final runout L^* with the column kinetics according to (4.1). Here, $E_K^U = MU^2/2$ is the column kinetic energy during the steady propagation, $M = L_0 H_0 \phi_0 \rho_s$ is the column mass with unitary width, and ϕ_0 is the initial column packing fraction. This scaling is compared with previous experimental and numerical results (Bougouin & Lacaze 2018; Polanía *et al.* 2022). The horizontal error bars show the variability associated with U. The dashed line follows a trend of power index 1.

Although polydispersity is not explicit in the model formulation, the initial packing fraction ϕ_0, which depends on it, is indispensable for obtaining the front kinetic energy. Note that the right-hand side of (4.1) is not dimensionless, but with this formulation the collapse energy becomes the principal variable that links the mobility of gravity-driven flows, condensing all the data into a trend with power index $\sim$1 (see inset in figure 10).

We understand that this model is an oversimplification of a complex physical process, but it is remarkable that the model can effectively link the final runout to the collapse kinematics across various levels of polydispersity and for both dry and immersed collapses. Notably, this model does not depend on fitting coefficients, and it needs only material parameters (i.e. ρ_s and ρ_f) and physically based variables (i.e. L_0, H_0, ϕ and U). The fact that results from two distinct methodologies and from experimental studies conducted by different authors align with the same trend suggests the possibility of a universal model. If it is found that this simplified model can be used to establish a universal link between the collapse mobility and kinematics, then it may prove useful in analysing and understanding mass movements such as landslides or debris flows, in areas where the only available data are the mobility and an interpretation of the initial geometry (Prada-Sarmiento *et al.* 2019).

5. Conclusions

We conducted an experimental study of dry and immersed dense granular column collapses. We varied the column height, ranging from short to tall columns, as well as the columns' grain size distribution from monodisperse to highly polydisperse systems, in order to assess the effect of the grain size distribution on the column collapse. The collapse sequence was analysed by means of image analysis and direct measurements of the basal pore fluid pressures, providing unique insight into the coupled kinematics of grains and fluid until the system comes to rest.

We have shown that the level of polydispersity has a stronger effect on immersed columns than on dry columns. For dry columns, the collapse sequence remains

independent of the polydispersity level, reaching similar distances at similar times. This observation is common for short and tall columns. The final runout of dry columns increases weakly with the polydispersity level. In immersed columns, the increase of the packing fraction, associated with an increase of the polydispersity level, plays an important role, most notably in the collapse initiation and in determining the runout distance. We observed that variations of these two features are caused by differences in the evolution of the pore pressures beneath the moving mass. In the column collapse initiation, there is a negative change of the pore pressure that induces a temporal increase of the column's strength. We showed that the collapse of polydisperse columns, with large packing fraction and low permeability, is delayed because the negative change of pore pressure has a greater amplitude and remains for a longer period than in monodisperse columns. Then, during the horizontal spreading stage of immersed collapses, the grain's deposition expels fluid from the moving mass and produces an excess, the same as a positive change, of the pore pressure. We revealed that in monodisperse collapses, the excess pore pressure is dissipated rapidly. In contrast, for polydisperse collapses, the large increase of the packing fraction means that the excess pore pressure remains for a longer period, decreasing the strength and producing a localised fluidisation that results in longer runout distances.

We confirmed that the link between the collapse energy during the propagation stage and the column mobility remains valid for three-dimensional processes, and works satisfactorily for dry and immersed collapses. The model is an oversimplification of a complex physical process, but it is remarkable that it scales the final runout with the collapse kinematics for a wide range of polydispersity levels. Moreover, this model collapses numerical and experimental results onto the same curve, suggesting that it might capture a universal scaling.

The findings of this work shed light on the effect that an increasing packing fraction, induced by an increasing polydispersity level, has on granular flows, and show that immersed flows depend strongly on the polydispersity level. Our results suggest that the packing fraction may be a better descriptor than a characteristic diameter in polydisperse granular flows. Our experimental work provides novel insight into the basal pore pressure variations and the influence that these have on the collapse sequence of immersed granular flows. Further studies might enrich our understanding of these complex systems, exploring other details such as the effects that cohesive granular contacts, grains with varying density or grain shape have on immersed flows.

Supplementary material and movies. Supplementary material and movies are available at https://doi.org/10.1017/jfm.2024.176.

Acknowledgements. We thank L. Lacaze for his stimulating thoughts and discussion, and thank him and A. Bougouin for sharing with us their experimental data to enrich and strengthen our study. We acknowledge the support of J. Monroy, J. Naranjo, M. Tobar and all the technical team in the hydraulic and geotechnical lab at Universidad de los Andes. Moreover, we would like to thank the anonymous referees for their valuable and constructive comments.

Declaration of interests. The authors report no conflict of interest.

Author ORCIDs.
Oscar Polanía https://orcid.org/0000-0003-4644-8989;
Nicolas Estrada https://orcid.org/0000-0003-4941-6253;
Emilien Azéma https://orcid.org/0000-0001-8831-3842;
Mathieu Renouf https://orcid.org/0000-0002-4362-3510;
Miguel Cabrera https://orcid.org/0000-0002-9236-8130.

References

Ahmed, S.S., Martinez, A. & DeJong, J.T. 2023 Effect of gradation on the strength and stress-dilation behavior of coarse-grained soils in drained and undrained triaxial compression. *J. Geotech. Geoenviron. Engng* **149** (5), 04023019.

Balmforth, N.J. & Kerswell, R.R. 2005 Granular collapse in two dimensions. *J. Fluid Mech.* **538**, 399–428.

Bougouin, A. & Lacaze, L. 2018 Granular collapse in a fluid: different flow regimes for an initially dense-packing. *Phys. Rev. Fluids* **3**, 064305.

Bougouin, A., Lacaze, L. & Bonometti, T. 2017 Collapse of a neutrally buoyant suspension column: from Newtonian to apparent non-Newtonian flow regimes. *J. Fluid Mech.* **826**, 918–941.

Breard, E.C.P., Dufek, J., Fullard, L. & Carrara, A. 2020 The basal friction coefficient of granular flows with and without excess pore pressure: implications for pyroclastic density currents, water-rich debris flows, and rock and submarine avalanches. *J. Geophys. Res. Solid Earth* **125** (12), e2020JB020203.

Breard, E.C.P., Dufek, J. & Roche, O. 2019 Continuum modeling of pressure-balanced and fluidized granular flows in 2-D: comparison with glass bead experiments and implications for concentrated pyroclastic density currents. *J. Geophys. Res. Solid Earth* **124** (6), 5557–5583.

Cabrera, M. & Estrada, N. 2019 Granular column collapse: analysis of grain-size effects. *Phys. Rev.* E **99**, 012905.

Cabrera, M. & Estrada, N. 2021 Is the grain size distribution a key parameter for explaining the long runout of granular avalanches? *J. Geophys. Res. Solid Earth* **126** (9), e2021JB022589.

Cantor, D., Azéma, E. & Preechawuttipong, I. 2020 Microstructural analysis of sheared polydisperse polyhedral grains. *Phys. Rev.* E **101**, 062901.

Cantor, D., Azéma, E., Sornay, P. & Radjai, F. 2018 Rheology and structure of polydisperse three-dimensional packings of spheres. *Phys. Rev.* E **98**, 052910.

Carman, P.C. 1937 Fluid flow through granular beds. *Chem. Engng Res. Des.* **75**, S32–S48.

Courrech du Pont, S., Gondret, P., Perrin, B. & Rabaud, M. 2003 Granular avalanches in fluids. *Phys. Rev. Lett.* **90**, 044301.

Dahl, S.R., Clelland, R. & Hrenya, C.M. 2003 Three-dimensional, rapid shear flow of particles with continuous size distributions. *Powder Technol.* **138** (1), 7–12, World Congress of Particle Technology.

Degaetano, M., Lacaze, L. & Phillips, J.C. 2013 The influence of localised size reorganisation on short-duration bidispersed granular flows. *Eur. Phys. J.* E **36**, 1–9.

Di Felice, R. 1994 The voidage function for fluid–particle interaction systems. *Intl J. Multiphase Flow* **20** (1), 153–159.

Gee, M.J.R., Masson, D.G., Watts, A.B. & Allen, P.A. 1999 The Saharan debris flow: an insight into the mechanics of long runout submarine debris flows. *Sedimentology* **46**, 317–335.

Gray, J.M.N.T. & Ancey, C. 2011 Multi-component particle-size segregation in shallow granular avalanches. *J. Fluid Mech.* **678**, 535–588.

Guo, X., Stoesser, T., Zheng, D., Luo, Q., Liu, X. & Nian, T. 2023 A methodology to predict the run-out distance of submarine landslides. *Comput. Geotech.* **153**, 105073.

He, K., Shi, H. & Yu, X. 2021 An experimental study on aquatic collapses of bidisperse granular deposits. *Phys. Fluids* **33** (10), 103311.

Ilstad, T., Marr, J.G., Elverhøi, A. & Harbitz, C.B. 2004 Laboratory studies of subaqueous debris flows by measurements of pore–fluid pressure and total stress. *Mar. Geol.* **213** (1), 403–414.

Iverson, R.M. 1997 The physics of debris flows. *Rev. Geophys.* **35** (3), 245–296.

Iverson, R.M. 2005 Regulation of landslide motion by dilatancy and pore pressure feedback. *J. Geophys. Res. Earth Surf.* **110** (F2), F02015.

Jop, P., Forterre, Y. & Pouliquen, O. 2005 Crucial role of sidewalls in granular surface flows: consequences for the rheology. *J. Fluid Mech.* **541**, 167–192.

Kaitna, R., Palucis, M.C., Yohannes, B., Hill, K.M. & Dietrich, W.E. 2016 Effects of coarse grain size distribution and fine particle content on pore fluid pressure and shear behavior in experimental debris flows. *J. Geophys. Res. Earth Surf.* **121** (2), 415–441.

Lacaze, L., Bouteloup, J., Fry, B. & Izard, E. 2021 Immersed granular collapse: from viscous to free-fall unsteady granular flows. *J. Fluid Mech.* **912**, A15.

Lai, Z., Vallejo, L.E., Zhou, W., Ma, G., Espitia, J.M., Caicedo, B. & Chang, X. 2017 Collapse of granular columns with fractal particle size distribution: implications for understanding the role of small particles in granular flows. *Geophys. Res. Lett.* **44** (24), 12181–12189.

Lajeunesse, E., Monnier, J.B. & Homsy, G.M. 2005 Granular slumping on a horizontal surface. *Phys. Fluids* **17** (10), 103302.

Lee, C.-H. 2021 Two-phase modelling of submarine granular flows with shear-induced volume change and pore-pressure feedback. *J. Fluid Mech.* **907**, A31.

Lube, G., Huppert, H.E., Sparks, R.S.J. & Hallworth, M.A. 2004 Axisymmetric collapses of granular columns. *J. Fluid Mech.* **508**, 175–199.

Martinez, F., Tamburrino, A., Casis, V. & Ferrer, P. 2022 Segregation effects on flow's mobility and final morphology of axisymmetric granular collapses. *Granul. Matt.* **24** (4), 101.

Meruane, C., Tamburrino, A. & Roche, O. 2010 On the role of the ambient fluid on gravitational granular flow dynamics. *J. Fluid Mech.* **648**, 381–404.

Meruane, C., Tamburrino, A. & Roche, O. 2012 Dynamics of dense granular flows of small-and-large-grain mixtures in an ambient fluid. *Phys. Rev.* E **86**, 026311.

Nguyen, D.-H., Azéma, E., Radjai, F. & Sornay, P. 2014 Effect of size polydispersity versus particle shape in dense granular media. *Phys. Rev.* E **90**, 012202.

Nguyen, D.-H., Azéma, E., Sornay, P. & Radjai, F. 2015 Effects of shape and size polydispersity on strength properties of granular materials. *Phys. Rev.* E **91**, 032203.

Oquendo-Patiño, W.F. & Estrada, N. 2022 Finding the grain size distribution that produces the densest arrangement in frictional sphere packings: revisiting and rediscovering the century-old Fuller and Thompson distribution. *Phys. Rev.* E **105**, 064901.

Pailha, M., Nicolas, M. & Pouliquen, O. 2008 Initiation of underwater granular avalanches: influence of the initial volume fraction. *Phys. Fluids* **20** (11), 111701.

Phillips, J.C., Hogg, A.J., Kerswell, R.R. & Thomas, N.H. 2006 Enhanced mobility of granular mixtures of fine and coarse particles. *Earth Planet. Sci. Lett.* **246** (3), 466–480.

Pinzon, G. & Cabrera, M. 2019 Planar collapse of a submerged granular column. *Phys. Fluids* **31** (8), 086603.

Pinzón, G. & Cabrera, M.A. 2019 Submerged planar granular column collapse: fluid fluxes at the collapsing granular front. In *Proceedings of the Seventh International Conference on Debris-Flow Hazards Mitigation*, special publication 28. Association of Environmental and Engineering Geologists.

Polanía, O., Cabrera, M., Renouf, M. & Azéma, E. 2022 Collapse of dry and immersed polydisperse granular columns: a unified runout description. *Phys. Rev. Fluids* **7**, 084304.

Polanía, O., Cabrera, M., Renouf, M., Azéma, E. & Estrada, N. 2023 Grain size distribution does not affect the residual shear strength of granular materials: an experimental proof. *Phys. Rev.* E **107**, L052901.

Prada-Sarmiento, L.F., Cabrera, M.A., Camacho, R., Estrada, N. & Ramos-Cañón, A.M. 2019 The Mocoa Event on March 31 (2017): analysis of a series of mass movements in a tropical environment of the Andean-Amazonian Piedmont. *Landslides* **16**, 2459–2468.

Rauter, M. 2021 The compressible granular collapse in a fluid as a continuum: validity of a Navier–Stokes model with $\mu(j)$, $\phi(j)$-rheology. *J. Fluid Mech.* **915**, A87.

Roche, O., Attali, M., Mangeney, A. & Lucas, A. 2011 On the run-out distance of geophysical gravitational flows: insight from fluidized granular collapse experiments. *Earth Planet. Sci. Lett.* **311** (3), 375–385.

Roche, O., Gilbertson, M.A., Phillips, J.C. & Sparks, R.S.J. 2005 Inviscid behaviour of fines-rich pyroclastic flows inferred from experiments on gas–particle mixtures. *Earth Planet. Sci. Lett.* **240** (2), 401–414.

Rondon, L., Pouliquen, O. & Aussillous, P. 2011 Granular collapse in a fluid: role of the initial volume fraction. *Phys. Fluids* **23** (7), 073301.

Sarlin, W., Morize, C., Sauret, A. & Gondret, P. 2021 Collapse dynamics of dry granular columns: from free-fall to quasistatic flow. *Phys. Rev.* E **104**, 064904.

Scott, G.D. 1960 Packing of spheres: packing of equal spheres. *Nature* **188** (4754), 908–909.

Staron, L. & Hinch, E.J. 2005 Study of the collapse of granular columns using two-dimensional discrete-grain simulation. *J. Fluid Mech.* **545**, 1–27.

Staron, L. & Hinch, E.J. 2007 The spreading of a granular mass: role of grain properties and initial conditions. *Granul. Matt.* **9**, 205–217.

Sufian, A., Knight, C., O'Sullivan, C., van Wachem, B. & Dini, D. 2019 Ability of a pore network model to predict fluid flow and drag in saturated granular materials. *Comput. Geotech.* **110**, 344–366.

Thompson, E.L. & Huppert, H.E. 2007 Granular column collapses: further experimental results. *J. Fluid Mech.* **575**, 177–186.

Topin, V., Monerie, Y., Perales, F. & Radjaï, F. 2012 Collapse dynamics and runout of dense granular materials in a fluid. *Phys. Rev. Lett.* **109**, 188001.

Wang, C., Wang, Y., Peng, C. & Meng, X. 2017 Dilatancy and compaction effects on the submerged granular column collapse. *Phys. Fluids* **29** (10), 103307.

WARNETT, J.M., DENISSENKO, P., THOMAS, P.J., KIRACI, E. & WILLIAMS, M.A. 2014 Scalings of axisymmetric granular column collapse. *Granul. Matt.* **16**, 115–124.

WATANABE, D., MORIGUCHI, S. & TERADA, K. 2022 A numerical study on the effects of particle size distribution on run-out distance of granular flow. *Soils Found.* **62** (6), 101242.

YANG, G.C., JING, L., KWOK, C.Y. & SOBRAL, Y.D. 2020 Pore-scale simulation of immersed granular collapse: implications to submarine landslides. *J. Geophys. Res. Earth Surf.* **125** (1), e2019JF005044.

ZENIT, R. 2005 Computer simulations of the collapse of a granular column. *Phys. Fluids* **17** (3), 031703.